Ding et al. Nanoscale Research Letters (2019) 14:157
https://doi.org/10.1186/s11671-019-2956-4

Nanoscale Research Letters

NANO EXPRESS Open Access

Low-Power Resistive Switching Characteristic in HfO_2/TiO_x Bi-Layer Resistive Random-Access Memory

Xiangxiang Ding, Yulin Feng, Peng Huang*, Lifeng Liu* and Jinfeng Kang

Abstract

Resistive random-access memory devices with atomic layer deposition HfO_2 and radio frequency sputtering TiO_x as resistive switching layers were fabricated successfully. Low-power characteristic with 1.52 μW set power (1 μA@1.52 V) and 1.12 μW reset power (1 μA@1.12 V) was obtained in the HfO_2/TiO_x resistive random-access memory (RRAM) devices by controlling the oxygen content of the TiO_x layer. Besides, the influence of oxygen content during the TiO_x sputtering process on the resistive switching properties would be discussed in detail. The investigations indicated that "soft breakdown" occurred easily during the electrical forming/set process in the HfO_2/TiO_x RRAM devices with high oxygen content of the TiO_x layer, resulting in high resistive switching power. Low-power characteristic was obtained in HfO_2/TiO_x RRAM devices with appropriately high oxygen vacancy density of TiO_x layer, suggesting that the appropriate oxygen vacancy density in the TiO_x layer could avoid "soft breakdown" through the whole dielectric layers during forming/set process, thus limiting the current flowing through the RRAM device and decreasing operating power consumption.

Keywords: RRAM, Low power, Atomic layer deposition, Titanium oxide

Introduction

Resistive random-access memory (RRAM) provides a promising solution for scaling down beyond traditional charge-based memory due to simple cell structure, non-volatile storage, high-speed operation, and high on/off ratio [1–10]. Recently, One-transistor one-resistor (1T1R) is a widely accepted structure to prevent inaccurate resistance measurements caused by a sneak path current in 1R array [11, 12]. Besides, the emerging memory, especially oxide-based RRAM, has been proposed for plastic synaptic devices due to the gradual conductance modulation with pulse number, which can mimic biological synaptic behavior to receive signals from pre- and postsynaptic neuron [13–17]. However, high resistive switching current is the main limitation for low-power and high-density application [18–20]. The 1T1R array also faces scaling challenges if the operation current of RRAM cannot scale accordingly. For example, when the CMOS technology is scaling down to 27 nm, the drive current will decrease to 40 μA [21]. Therefore, reducing operation current of RRAM device down to 10 μA by optimizing structure and material is necessary to continue 1T1R scaling [22]. In addition, biological synapses consume around 1 ~ 10 fJ per event in the complex human brain, thus, reducing the energy consumption of electrical synaptic devices as little as biological synapses is important for the development of neuromorphic artificial neural networks (ANNs) [23–25]. Therefore, limiting the device current and reducing the power consumption will benefit the practical process for data storage and neuromorphic computing application.

In this work, $Pt/HfO_2/TiO_x/Pt$ devices with a different oxygen content of TiO_x film were fabricated, and low-power characteristic in low oxygen content was demonstrated. The memory device achieved 1.52 μW set power and 1.12 μW reset power through decreasing oxygen content of the TiO_x film during the sputtering process. The conductive mechanism for low-power char-

* Correspondence: phwang@pku.edu.cn; lfliu@pku.edu.cn
Institute of Microelectronics, Peking University, Beijing 100871, China

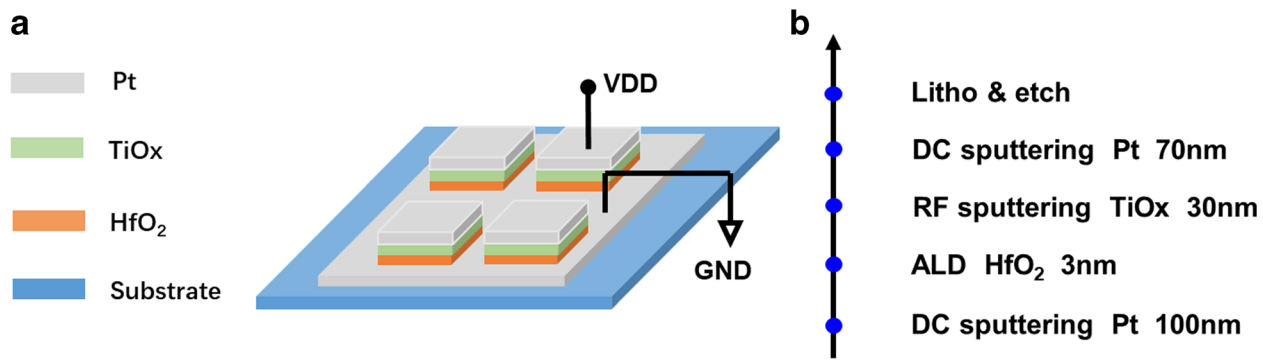

Fig. 1 **a** The structure of Pt/HfO2/TiO_x/Pt device. **b** The fabrication process flow

acteristic was analyzed further to provide insights into oxide RRAM design.

Methods

The Pt/HfO_2/TiO_x/Pt device structure and fabrication process are shown in Fig. 1a and b. At first, on Si/SiO_2/Ti substrate, a 100-nm Pt bottom electrode (BE) was prepared by direct current (DC) sputtering at room temperature. Next, 3 nm HfO_2 was deposited by atomic layer deposition (ALD) (Picosun R200) technique at 300 °C using TEMAH and H_2O as precursors. Subsequently, 30 nm TiO_x was deposited with different oxygen content by radio frequency sputtering. During TiO_x film sputtering process, fixing the total gas flow of argon (Ar) and oxygen (O_2) as 20 sccm and changing the oxygen partial pressure with 9%, 11%, and 13%, three sample devices (S1, S2, and S3) were obtained to investigate the influence of oxygen content of TiO_x film on the resistive switching performance. Following that, a 70-nm Pt top electrode (TE) was deposited by DC sputtering and patterned with lithography. Finally, 100 μm × 100 μm square-shape devices were formed by reactive ion etching (RIE). Bias voltage was applied on the TE, and the BE was connected with the ground. The high-resolution transmission electron microscope (HRTEM) images of the cross-section of the Pt/HfO_2/TiO_x/Pt are shown in Fig. 2. The electrical characteristics of the devices were measured with Agilent B1500A semiconductor parameter analyzer. The chemical states of atoms in the TiO_x films were investigated by X-ray photoelectron spectroscopy (XPS, Axis Ultra).

Results and Discussion

Figure 3a, b, and c show the XPS O 1s core-level spectra of TiO_x films. To clarify the chemical bond of oxygen in the films, the asymmetric O 1s peaks are divided into two peaks, which are generally ascribed to the O^{2-} bonded by metal ions and O^{2-} in the oxygen-deficient region [26]. Oxygen partial pressure during TiO_x film sputtering process was set as 9%, 11%, and 13%,

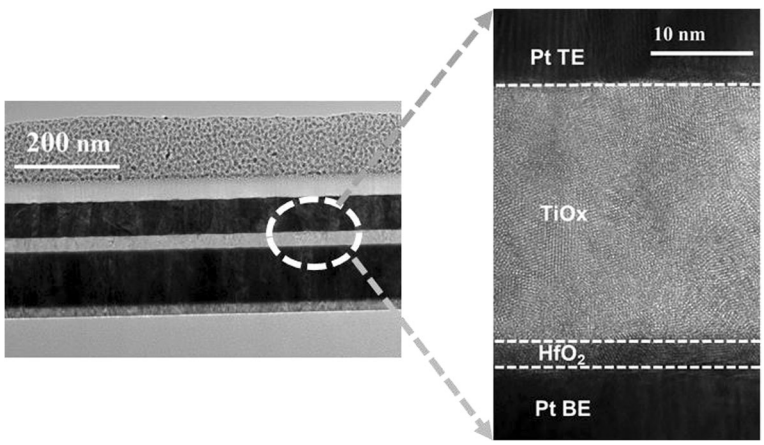

Fig. 2 TEM cross-sections of the Pt/HfO_2/TiO_x/Pt device

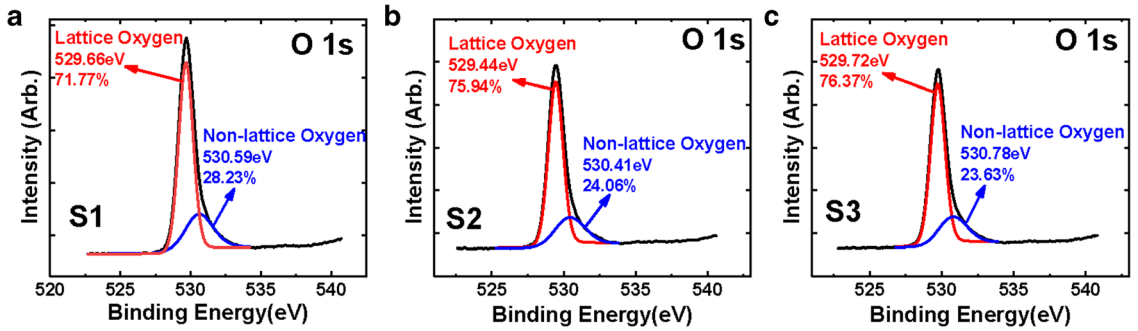

Fig. 3 O 1s XPS scan spectra of TiO_x films in S1, S2, and S3. Oxygen partial pressure was set as **a** 9%, **b** 11%, and **c** 13% during TiO_x film sputtering process

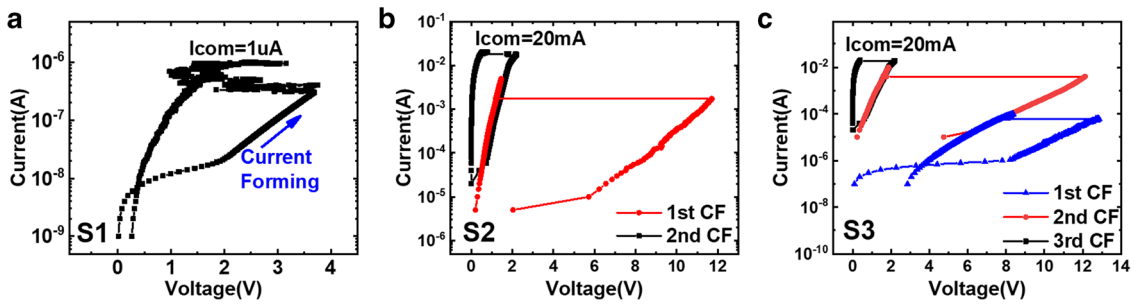

Fig. 4 Current forming process of the Pt/HfO2/TiO_x/Pt RRAM device in **a** S1, **b** S2, and **c** S3

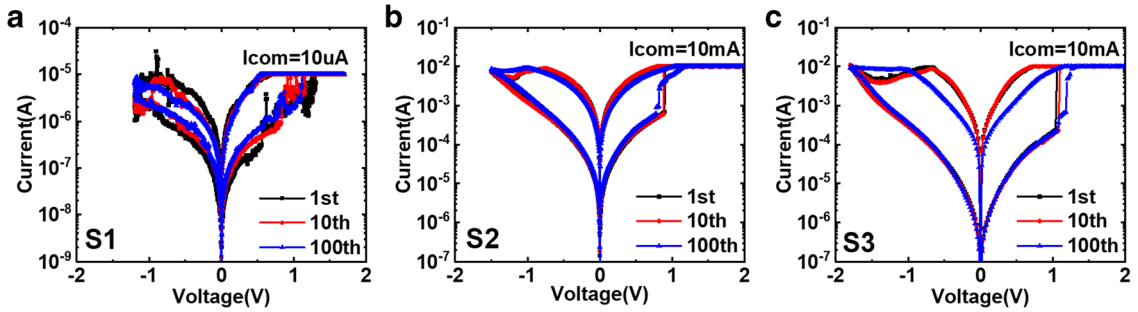

Fig. 5 100 cycles stable bidirectional I-V curves in **a** S1, **b** S2, and **c** S3

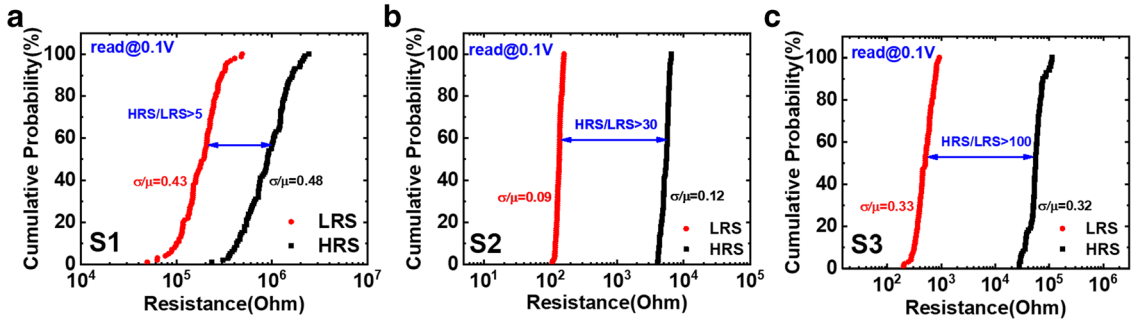

Fig. 6 Cycle-to-cycle variation of R_{LRS} and R_{HRS} for 100 cycles in **a** S1, **b** S2, and **c** S3

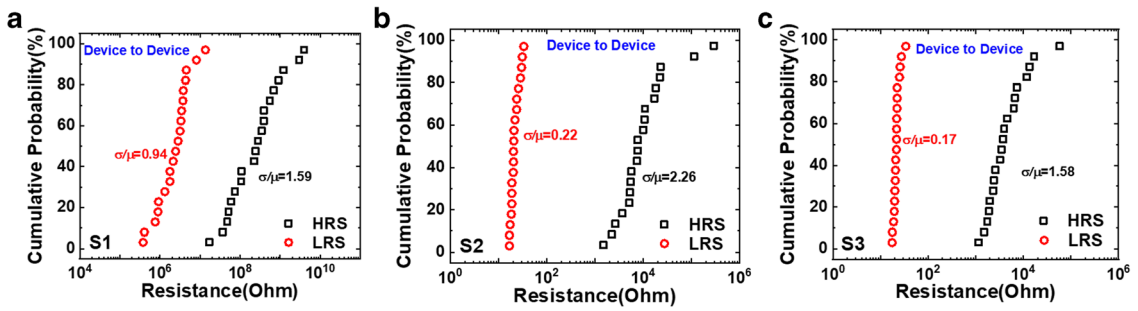

Fig. 7 Device-to-device variation of R_{LRS} and R_{HRS} for 20 devices in **a** S1, **b** S2, and **c** S3

respectively, and the corresponding oxygen-deficient content in three samples is about 28.23%, 24.06%, and 23.63%, indicating that the content of non-lattice oxygen ions and oxygen vacancies decreases with increasing oxygen partial pressure.

For the fresh devices, the original state is in high resistance state (HRS). As shown in Fig. 4, current forming (CF) is applied to initiate the formation of the conductive filament and change the device state to low resistance state (LRS) [27]. When applying 1 μA of current compliance, a conductive path is formed in S1 and the stable set/reset process can be achieved in the subsequent operation. For S2 and S3, reset operation is not successful from the middle state of the device during CF process until the current compliance is up to 20 mA.

In order to test the electrical performance of the RRAM device, DC measurements under voltage sweep are carried out. Positive bias voltage in forming and set process is applied on TE to complete the conductive filament, and negative bias voltage in reset process is to break the filament. When the bias is swept back and forth, 100 cycles of bipolar switching current-voltage (I-V) curves of three samples are shown in Fig. 5. The S1 devices achieve stable resistive switching performance under 10 μA current compliance, but the operation current is up to 10 mA for the other two samples. The low-power characteristic of S1 could be attributed to high oxygen vacancy content preexisting in TiO_x film, which limits the current effectively during forming/set process.

Figures 6 and 7 depict the cycle-to-cycle and device-to-device variation (relative standard deviation, (σ/μ)) of three samples, and the statistics are summarized in Tables 1 and 2. For S1, weak hopping current causes modest resistance distribution, and the strong conductive filaments formed in S2 and S3 guarantee the relatively stable resistance distribution. Although there is a little degradation for S3 after dozens of cycles, the on/off ratio is still over 100.

As shown in Fig. 8, the set power (Pset) 1.52 μW and the reset power (Preset) 1.12 μW are reached under a low compliance current of 1 μA. The power consumption of the other two samples is tens of milliwatt due to 10 mA of operation current. Besides, the resistance states of S1 can keep retention characteristics over 10^4 s under 85 °C with approximate 100 on/off ratio, which is stable for data storage application.

To elucidate the conductive mechanism of low-power characteristic, we carried out temperature measurements for S1 and S3 with different operation current and investigated the corresponding mechanism, as shown in Figs. 9 and 10. From 25 °C to 125 °C, the resistance of S1 decreases with temperature, but the resistance of S3 almost does not change. The experimental conductance and temperature are fitted with Mott's variable range hopping model [28], as shown as Fig. 11, which indicates that the main conductive mechanism of S1 is electrons hopping via localized oxygen vacancy defects in dielectric oxide [29]. When decreasing the oxygen

Table 1 The cycle-to-cycle variation characteristic of three samples

Sample	Average value(μ) (ohm)		Standard deviation(σ) (ohm)		Relative standard deviation (σ/μ)	
	LRS	HRS	LRS	HRS	LRS	HRS
S1	1.96e5	9.91e5	8.35e4	4.80e5	0.43	0.48
S2	134.75	5.35e3	12.13	663.24	0.09	0.12
S3	520.12	5.83e4	170.40	1.85e4	0.33	0.32

Table 2 The device-to-device variation characteristic of three samples

Sample	Average value(μ) (ohm)		Standard deviation(σ) (ohm)		Relative standard deviation(σ/μ)	
	LRS	HRS	LRS	HRS	LRS	HRS
S1	3.20e6	6.28e8	2.99e6	9.96e8	0.94	1.59
S2	22.32	2.90e4	4.83	6.56e4	0.22	2.26
S3	22.09	7.61e3	3.67	1.20e4	0.17	1.58

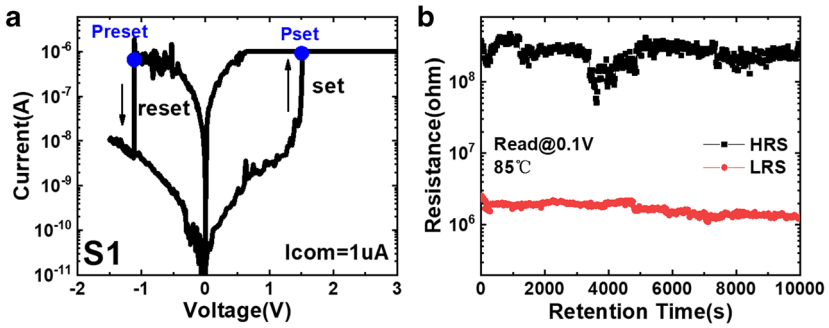

Fig. 8 a Resistive switching performance under 1 μA current limitation. **b** Retention characteristic in S1 is over 10^4 s under 85 °C

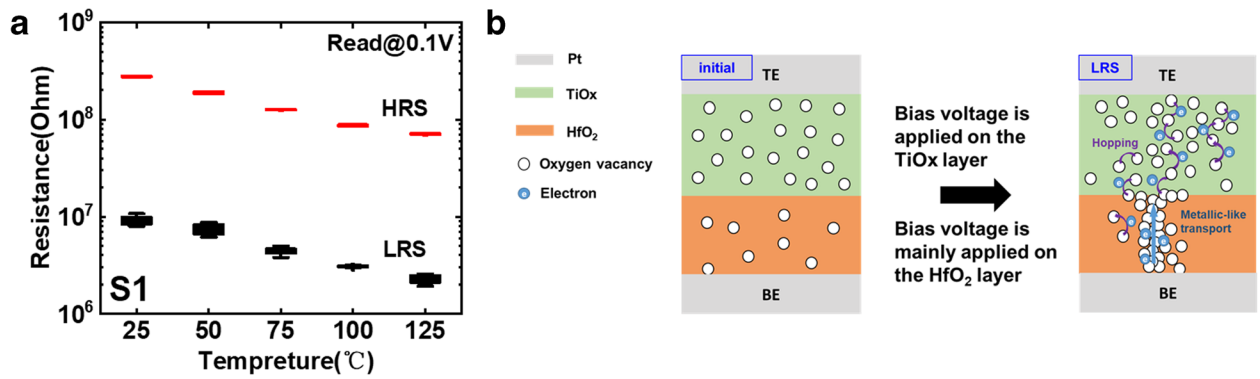

Fig. 9 a The resistance changes with temperature in S1. **b** The corresponding schematic diagram of conductive mechanism

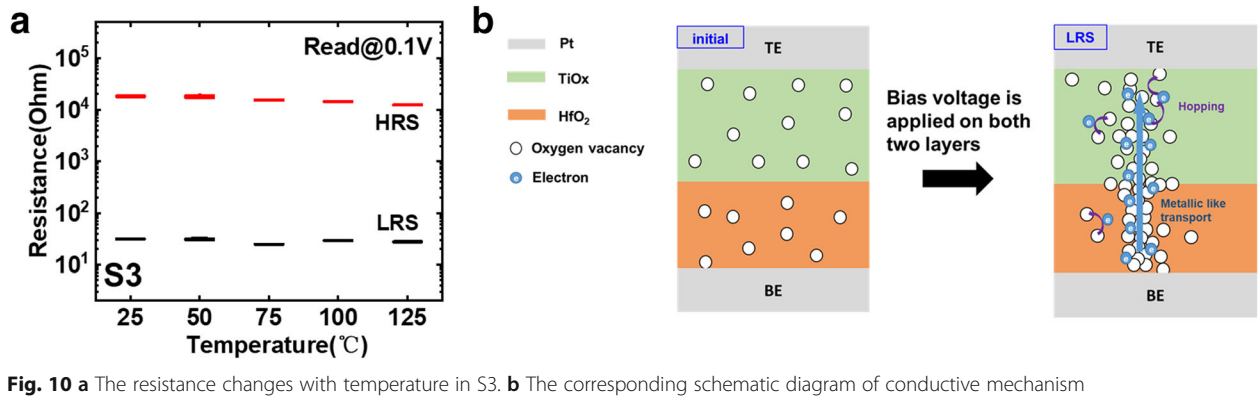

Fig. 10 a The resistance changes with temperature in S3. **b** The corresponding schematic diagram of conductive mechanism

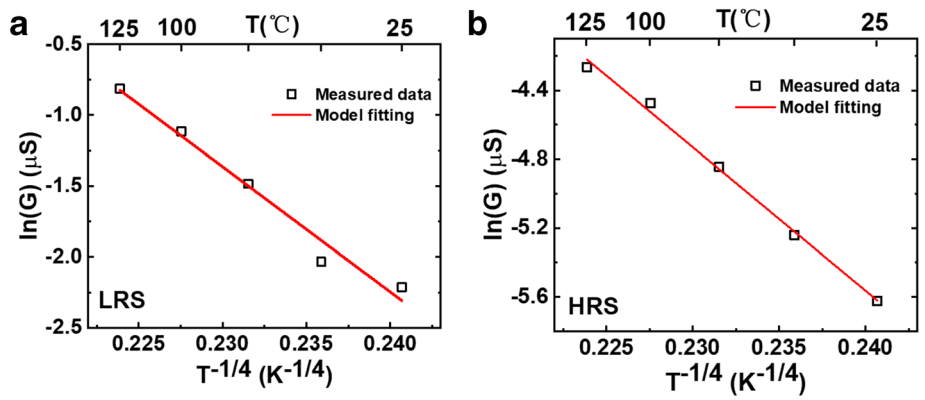

Fig. 11 Temperature dependence of the conductance of S1 in **a** LRS and **b** HRS

partial pressure during the TiO_x sputtering process, as shown in S1, the oxygen vacancy content in initial TiO_x layer increases and the film resistance decreases [30]. The voltage on the TE is applied mainly on the HfO_2 layer and a mass of oxygen vacancies are motivated to form the conductive filament. After that, new oxygen vacancies are also motivated in the TiO_x layer, but the connection among oxygen vacancies is weak. Therefore, electrons hopping conduction in TiO_x is dominant, which ensures low 1-μA resistive switching current.

However, as shown in Fig. 10, after increasing oxygen content during TiO_x sputtering process, HRS and LRS remain almost unchanged with temperature, which is most likely associated with the metallic-like transport mechanism, induced by electrons transport through conductive filament consisted of concentrated oxygen vacancies. Compared with the RRAM device of S1, fewer oxygen vacancies in initial TiO_x layer of S3 are not enough for electrons hopping conduction. Besides, due to the increased resistance of TiO_x film, the voltage bias is applied on both HfO_2 layer and TiO_x layer at the same time. Electric initialization leads to plenty of oxygen vacancies motivated in HfO_2 and TiO_x layers. These oxygen vacancies form a strong conductive filament in both two dielectric layers, and the abundant extended electrons flow through the two adjacent oxygen vacancies, which causes high operation current during resistive switching process.

In principle, it is possible to control oxygen content carefully to achieve low-power performance in other oxide resistive memories (OxRRAM) related to the oxygen vacancy. The requirement for the oxide layer is that there should be enough oxygen vacancies in the initial state for electrical hopping conduction in case of the device breakdown. However, the excessive oxygen vacancies will cause unstable endurance characteristic and deteriorate the device performance. Therefore, the appropriate oxygen vacancies are necessary to limit operation current and decrease power consumption.

Table 3 compares some of the key parameters of the $Pt/HfO_2/TiO_x/Pt$ device with other recent reports. The device has important merits of low 1.12 μW resistive switching power and over 100 HRS/LRS ratio among various RRAM devices.

Conclusions

In this work, 1-μA resistive switching current was demonstrated in $Pt/HfO_2/TiO_x/Pt$ structure device. For the conductive mechanism, electrons hopping conduction is dominant in low oxygen content of the TiO_x layer, which limits operation current and decreases power consumption. Metallic-like transport is dominant in high oxygen

Table 3 Comparison of device performance for RRAM devices

Device structure	Type	Iset@Vset	Ireset@Vreset	HRS/LRS	Pset, preset	Reference
$Pt/TiO_x/HfO_2/Pt$	OxRRAM	1 μA@1.52 V	1 μA@− 1.12 V	100	1.52 μW, 1.12 μW	This work
$Pt/C/Ta_2O_5/TiN$	OxRRAM	1 mA@− 1.5 V	0.3 mA@2.6 V	100	1.5 mW, 0.78 mW	[5]
$TiN/Ti/HfO_x/TiN$	VRRAM	100 μA@1.15 V	92 μA@− 0.98 V	10	115 μW, 90.2 μW	[6]
Cu/black phosphorus/Au	CBRAM	0.9 mA@0.71 V	0.9 mA@− 0.57 V	1000	0.64 mW, 0.51 mW	[7]
$Sn/HfO_2/Pt$	CBRAM	1 mA@3.5 V	6 mA@− 1.67 V	1e5	3.5 mW, 10.02 mW	[8]
Nb/NiO/Nb	Unipolar	15 mA@0.82 V	15 mA@0.38 V	100	12.3 mW, 5.7 mW	[9]
$Ta/Ta_2O_5/Pt$	Unipolar	1 mA@2.31 V	8 mA@1 V	20	2.31 mW, 8 mW	[10]

content of the TiO_x layer, and "soft-breakdown" of two dielectric layers causes high operation current and high power consumption. The appropriate oxygen content of TiO_x film can limit the RRAM current and contribute to low-power characteristic, which provides a solution for large operation current and high-power issues and shows the promise for future embedded non-volatile memories and the Internet of things (IoT) applications.

Abbreviations

1T1R: One-transistor one-resistor; ALD: Atomic layer deposition; ANNs: Artificial neural networks; BE: Bottom electrode; CF: Current forming; HRS: High resistance state; HRTEM: High-resolution transmission electron microscope; IoT: Internet of things; I-V: Current-voltage; LRS: Low resistance state; On/off ratio: HRS/LRS; OxRRAM: Oxide resistive memory; Preset: Reset power; Pset: Set power; RIE: Reactive ion etching; RRAM: Resistive random-access memory; TE: Top electrode; XPS: X-ray photoelectron spectroscopy; σ/μ: Relative standard deviation

Acknowledgements

This work was supported in part by the National Key Research and Development Program (2017YFB0405600), the National Natural Science Foundation of China (61421005, 61874006, 61334007 and 61834001) and the 111 Project (B18001).

Availability of Data and Materials

All data generated or analysed during this study are included in this published article.

Authors' Contributions

XD fabricated the RRAM devices; carried out the electrical measurements with the assistance of YF; and drafted the manuscript under the instruction of LL, PH, and JK. LL and JK supervised the work and finalized the manuscript. All authors had read and approved the final manuscript.

Competing Interests

The authors declare that they have no competing interests.

Publisher's Note

Received: 31 December 2018 Accepted: 22 March 2019
Published online: 09 May 2019

References

1. Wong HSP, Lee HY, Yu S et al (2012) Metal–oxide RRAM. Proc IEEE 100(6): 1951–1970
2. Kim YB, Lee SR, Lee D et al (2011) Bi-layered RRAM with unlimited endurance and extremely uniform switching. In: VLSI Technology, 2011 Symposium on. IEEE, pp 52–53
3. Li KS, Ho CH, Lee MT et al (2014) Utilizing sub-5 nm sidewall electrode technology for atomic-scale resistive memory fabrication. In: VLSI Technology: Digest of Technical Papers, 2014 Symposium on. IEEE, pp 1–2
4. Govoreanu B, Kar GS, Chen YY et al (2011) 10× 10nm 2 Hf/HfOx crossbar resistive RAM with excellent performance, reliability and low-energy operation. In: Electron Devices Meeting (IEDM), 2011 IEEE International. IEEE, pp 31.6. 1–31.6. 4
5. Schönhals A, Rosário CMM, Hoffmann-Eifert S et al (2018) ReRAM: role of the electrode material on the RESET limitation in oxide ReRAM devices. Adv Electron Mater 4(2):1870011
6. Li H, Li KS, Lin CH et al (2016) Four-layer 3D vertical RRAM integrated with FinFET as a versatile computing unit for brain-inspired cognitive information processing. In: VLSI Technology, 2016 Symposium on. IEEE, pp 1–2
7. Rehman S, Khan MF, Aftab S et al (2019) Thickness-dependent resistive switching in black phosphorus CBRAM. J Mater Chem C 7(3):725
8. Sonde S, Chakrabarti B, Liu Y et al (2018) Silicon compatible Sn-based resistive switching memory. Nanoscale 10:9441
9. Yoonho A, Wook SH, Hoon LT et al (2018) Effects of Nb nanopin electrode on resistive random-access memory switching characteristics of NiO thin films. Nanoscale. https://doi.org/10.1039/C8NR02986E
10. Gao S, Liu G, Chen Q et al (2018) Improving unipolar resistive switching uniformity with cone-shape conducting filaments and its logic-in-memory application. ACS Appl Mater Interfaces. https://doi.org/10.1021/acsami.7b19586
11. Su YT, Liu HW, Chen PH et al (2018) A method to reduce forming voltage without degrading device performance in hafnium oxide-based 1T1R resistive random access memory. IEEE J Electron Devices Soc 6(1):341–345
12. Wu MC, Lin YW, Jang WY et al (2011) Low-power and highly reliable multilevel operation in ZrO2 1T1R RRAM. IEEE Electron Device Lett 32(8): 1026–1028
13. Yu S (2018) Neuro-inspired computing with emerging nonvolatile memorys. Proc IEEE 106(2):260–285
14. Kim CH, Lim S, Woo SY et al (2018) Emerging memory technologies for neuromorphic computing. Nanotechnology 30(3):032001
15. Snider GS (2008) Spike-timing-dependent learning in memristive nanodevices. In: Proceedings of the 2008 IEEE International Symposium on Nanoscale Architectures. IEEE Computer Society, pp 85–92
16. Kuzum D, Yu S, Wong HSP (2013) Synaptic electronics: materials, devices and applications. Nanotechnology 24(38):382001
17. Markram H, Gerstner W, Sjöström PJ (2011) A history of spike-timing-dependent plasticity. Front Synaptic Neurosci 3:4
18. Cheng CH, Chin A, Yeh FS (2010) Novel Ultra-low power RRAM with good endurance and retention. In: VLSI Technology. IEEE, pp 85–86
19. Lee MJ, Lee CB, Lee D et al (2011) A fast, high-endurance and scalable non-volatile memory device made from asymmetric Ta_2O_{5-x}/TaO_{2-x} bilayer structures. Nat Mater 10(8):625
20. Mandal S, El-Amin A, Alexander K et al (2014) Novel synaptic memory device for neuromorphic computing. Sci Rep 4:5333
21. Zahurak J, Miyata K, Fischer M et al (2014) Process integration of a 27nm, 16Gb Cu ReRAM. In: Electron Devices Meeting (IEDM). IEEE
22. Yu S, Chen PY (2016) Emerging memory technologies: recent trends and prospects. IEEE Solid-State Circuits Mag 8(2):43–56
23. Yu S, Gao B, Fang Z et al (2013) A low energy oxide-based electronic synaptic device for neuromorphic visual systems with tolerance to device variation. Adv Mater 25(12):1774–1779
24. Drachman DA (2005) Do we have brain to spare? Neurology 64(12):2004–2005
25. Guizzo E (2011) IBM's Watson Jeopardy computer shuts down humans in final game. IEEE Spectr 17. https://spectrum.ieee.org/automaton/robotics/artificial-intelligence/ibm-watson-jeopardy-computer-shuts-down-humans
26. Veith GM, Lupini AR, Dudney NJ (2009) Role of pH in the formation of structurally stable and catalytically active TiO2-supported gold catalysts. J Phys Chem C 113(1):269–280
27. Gao B, Liu L, Liu X et al (2012) Resistive switching characteristics in HfOx layer by using current sweep mode. Microelectron Eng 94(none):14–17
28. Lin GR, Chen WC, Chang CS et al (1994) Electrical characterization of arsenic-ion-implanted semi-insulating GaAs by current-voltage measurement. Appl Phys Lett 65(25):3272–3274
29. Gao B, Kang JF, Chen YS et al (2011) Oxide-based RRAM: unified microscopic principle for both unipolar and bipolar switching. In: Electron Devices Meeting. IEEE
30. Bally AR, Hones P, Sanjinés R et al (1998) Mechanical and electrical properties of fcc TiO_{1+x} thin films prepared by r.f. reactive sputtering. Surf Coat Technol s 108–109(98):166–170